WAYS OF WORKING THE DATA OBTAINED THROUGH ATOMIC FORCE MICROSCOPY TECHNOLOGY

Marius Dan BENȚA[*], Cosmin AFRENȚOAEI[**], Eusebiu PAIU[**], Laurențiu TODORAN[**], Octavian DADU[**]

[*] Transilvania University of Brasov, Romania
[**] Transport Technical College Brasov, Romania

Abstract. The article presents a series of methods of working the data obtained through Atomic Force Microscopy technology. It shows the way in which the obtained data can be used and read through the Labview programming language. Emphasis is also laid on a series of advantages resulting from scanning by the direct contact or the non-contact method. AFM consists of a sharp microfabricated tip attached to a cantilever, which is scanned across a sample. The deflection of this cantilever is monitored using a laser and photodiode and is used to generate imaging or spectra of the surface. The AFM works in a number of different modes.

Keywords: technology, Atomic Force Microscopy

1. Introduction

Atomic Force Microscopy - AFM is a powerful surface analytical technique used in air, liquid or vacuum to generate very high-resolution images of a surface and can provide some topographic, chemical, mechanical, electrical information [7]. An AFM consists of a sharp microfabricated tip attached to a cantilever, which is scanned across a sample. The deflection of this cantilever is monitored using a laser and photodiode and is used to generate imaging or spectra of the surface. The AFM works in a number of different modes [7]. These include:

Contact mode - The tip is kept in constant contact with the sample (with a force range of 1-1000 nN, it may be used with hard materials) and provides the basic mode for topography [7];

Force modulation mode - The tip is kept in contact but a modulated signal is also applied which gives information on dynamic responses from surfaces. Phase and stiffness imaging are extracted from the modulated response signal. This is conducted in the frequency ranges of 10-20 kHz and 400-1000 kHz and modulation forces of around 100 pN - 500 nN [3];

Intermittent and non-contact imaging - The tip is oscillated normal to the surface enabling soft materials to be imaged for topography. This eliminates much of the shear force involved in the contact mode. Phase images are also taken in this mode [7];

Force versus distance spectroscopy - The AFM applies forces from 50 µN to 5 pN to one spot on a surface to analyse material mechanical properties at surfaces.

It either pushes into the surface to measure nanomechanical properties of a surface such as modulus and adhesion or pulls away from the surface for example to measure the forces associated with unfolding of proteins or the breaking of individual covalent bonds [7].

The hysteresis of the scanner can be controlled by use of closed-loop sensors. The deflection of the cantilever is measured using a laser and a position sensitive diode. The force acting on the sample is calculated from the product of the cantilever spring constant and the cantilever deflection.

The example below is a simple force-distance curve on a piece of silicon wafer [7].

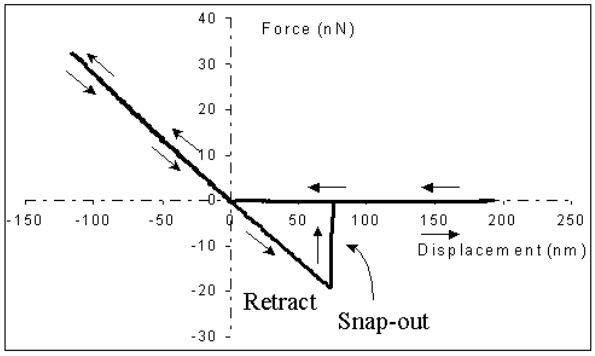

Figure 1. A simple AFM force-distance curve on a silicon wafer [15]

When a tip is far away from the surface no forces act, as the tip approaches a sample it experiences an attractive van der Waals force until it snaps onto the surface [7]. For studies in ambient conditions, this is promoted by a small neck of water, which condenses at very small separations. As the tip moves further, the cantilever is deflected by the sample. As the tip is withdrawn, the small capillary layer of water and organics on the sample surface hold the tip longer than expected until the snap-out point is reached. This snap-out displacement is dependent on several factors such as the tip size, and the nature of the surface and ambient environment [7].

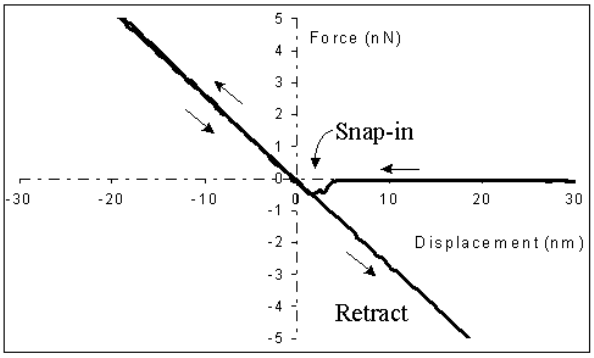

Figure 2. Zoomed in region of a force-distance curve showing the snap-in event [15]

Thermally sprayed coatings are now used extensively in a variety of applications. However, their application has often preceded detailed knowledge or understanding of their corrosion mechanisms or rates. Previous studies involving plasma sprayed coatings [7] have shown that good quality coatings, in terms of low porosity, are essential to protect the substrate from corrosion. There are many thermal spray processes available to date: the high velocity oxygen fuel (HVOF) process, which uses higher exhaust velocities and lower flame temperatures than other processes, can produce coatings of low porosity levels (1%) and avoids alteration of the mechanical properties of the substrate [4]. The corrosion characteristics of thermal sprayed coatings in static saline environments are extremely important where the flow of aqueous solution over components intermittently ceases. It has been established [1, 2] that where coatings are applied by a high-quality process and under stringent quality control procedures, the coatings can provide a very effective barrier to the substrate and prevent any corrosion from occurring. In this situation, however, it is very important to appreciate that corrosion of the coating can occur and that initiation and propagation of corrosion, associated with microstructural features of the composite system, are a real issue. For improvements to the coating corrosion resistance to be made, a full understanding of the corrosion rates and mechanisms, and in particular the resistance of the metallic binder (in cermet systems), is required. In addition, an understanding of static corrosion behaviour can help reveal the mechanisms of the coating degradation in erosion-corrosion environments [5, 6]. This article investigates the corrosion rates and mechanisms of two HVOF coatings (WC-Co-Cr and WC-Co).

2. Experimental procedure

Two HVOF sprayed coatings are studied in this work: a WCCo-Cr coating with nominal composition 86%WC10%Co-4% Cr, and a WC-Co coating with a nominal composition 86% WC-14% Co. The coatings were applied to a stainless steel substrate (UNS S31603). Specimens were soldered on the rear side to an electrical conducting wire and subsequently encapsulated in nonconducting resin. The exposed coated face of the specimen was then ground with silicon carbide abrasive papers and polished to a 6 μm diamond finish. The main seawater constituents were 19300 ppm chloride, 11000 ppm sodium, 2700 ppm sulfate, 1300 magnesium, 400 ppm calcium, 400 ppm potassium, and 150 ppm bicarbonate ions. The specimen-resin interfaces were sealed using Lacomit varnish (Agar Aids, UK) to prevent interference from the substrate. Electrochemical monitoring was carried out with a standard three-electrode cell, comprising a platinum auxiliary electrode and a saturated calomel reference electrode (SCE). Direct current (DC) anodic polarization tests were carried out after 1 h immersion in the seawater at 18 and 50 °C.

The seawater was left open to the atmosphere, figure 1.

Anodic polarization curves in static artificial seawater at 18 °C on WC-Co-Cr and WC-Co HVOF sprayed coatings The potentiostat was used to scan the electrode potential of the coating samples from the free corrosion potential (Ec o r r) in the positive (anodic) direction until a current in the range of 500-700 μA/cm2. In addition, an atomic force microscope (AFM) was used to map the topography of the coatings during accelerated corrosion tests. The AFM was configured to probe the surface under water and to record images during anodic polarization.

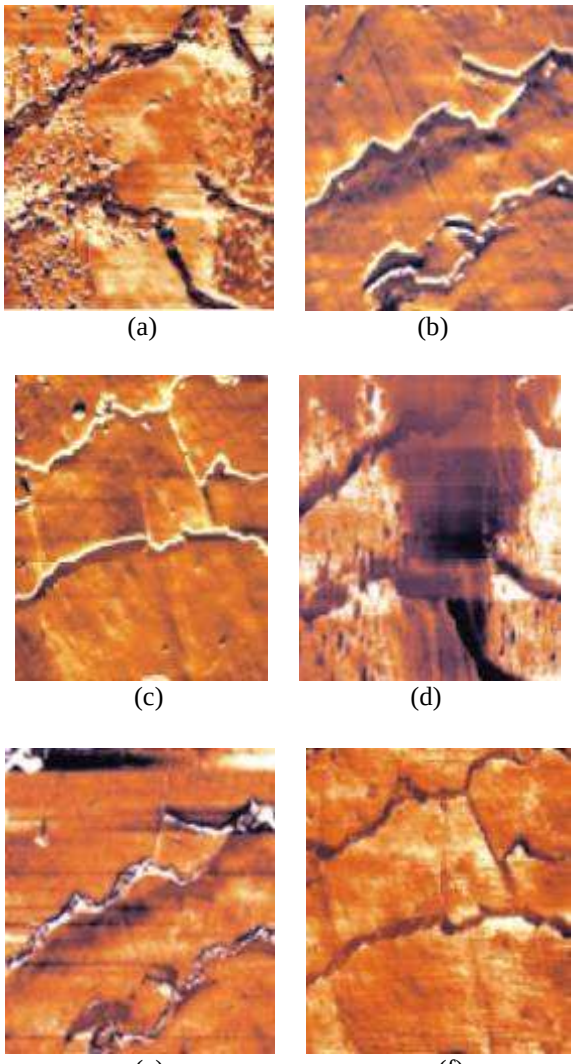

(a) (b) (c) (d) (e) (f)

Figure 3. In situ AFM images
(a) Polished coating prior to polarization; (b) points A to B; (c) points B to C; (d) points C to D; (e) points D to E; and (f) end of anodic polarization

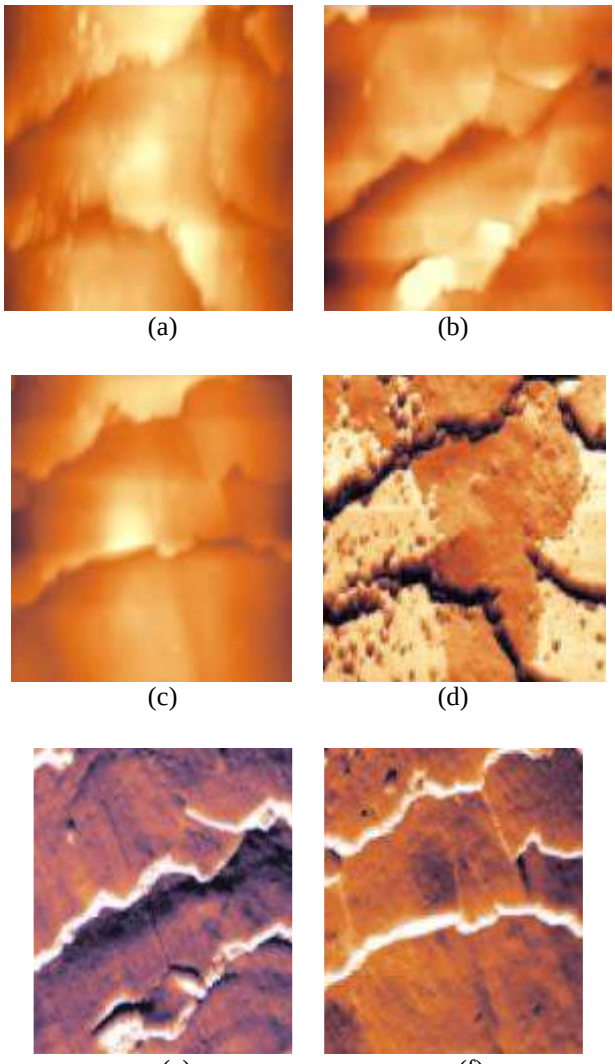

(a) (b) (c) (d) (e) (f)

Figure 4. In situ AFM images
(a) Polished coating prior to polarization; (b) point B; (c) point C; (d) point D; and (e) end of anodic polarization

Each image took 6 min. to produce, during which time the potential had shifted by approximately 90 mV.

3. Results

During the decrease in current (points B to C), the matrix is dissolving at a steady rate, defining the hard phase particles more clearly (figure 3c). As the current increases (points C to D in figure 3d), the matrix dissolves further, revealing the smaller hard phases from point D to E (figure 3e). At the end of the anodic polarization, areas where the matrix has dissolved in some regions and areas of attack around the matrix-hard phase interface can be seen (figure 3f).

In a similar manner, the corrosion mechanisms during anodic polarization of the WC-Co-Cr coating were examined.

Figure 4a shows the coating at the free corrosion potential with the light grey hard phases encased in the darker grey matrix. The rapid increase in current with the potential corresponds to dramatic matrix dissolution and leaves the hard phase protruding from the matrix (figure 4c).

As the current stabilizes at point D, carbides begin to fall out from the matrix and leave voids behind (figure 4d). These progresses until the end of the scan at point E, where the matrix consists mainly of voids left by the carbide particles and a few carbides on the next layer are visible (figure 3e). After immersion in seawater for 1 h at 50°C, the kinetics of the anodic polarization processes are accentuated on both coatings.

4. Conclusion

The use of an AFM can aid the determination of corrosion mechanisms on a microscale. The addition of chromium to a cobalt matrix increases the corrosion resistance of a WC-based HVOF sprayed cermet coating and its extent of this has been quantified. Although the WC-Co-Cr coating undergoes more localized attack at 18 °C, accentuated at the hard phase-matrix interface, the WC-Co has more uniform corrosion affecting the entire matrix. An increase in temperature results in extensive dissolution of the cobalt matrix, whereas on the CoCr matrix more severe attack is further localized in regions not associated with any specific microstructural features.

Acknowledgment

This research work is supported by The National Authority for Scientific Research (CNCSIS Romania): Grant CNCSIS, PN – II – ID – PCE – 2008, code 2291: "Laser Radiation – Substance Interaction: Physical Phenomena, Modelling and Techniques of Electromagnetic Polluation Rejection".

References

1. Tsai, S.T., Shih, H.C. (2007) *The Use of Thermal-Spray Coatings for Preventing Wet H2S Cracking in HSLA Steel Plates*. Corros. Prev. Control, no. 44, p. 42-48
2. Duncan, R.J., Thompson, C.B. (1991) *A Guide to Weld and Thermal Spray Hardfacing in the Pulp and Paper Industry. Part 2: Applications. Mater*. Des., 1991, no. 11, p. 71-75
3. Binnig G., Quate C.F., Gerber Ch. (1986) *Atomic force microscope*, Phys. Rev. Lett. no. 56, p. 930-933
4. Drozdov, M., Gur, G., Atzmon, Z., Kaplan, W.D. (2007) Microstructural *Evaluation of Al-Cu Intermetallic Phases in Wire-Bonding*. Available from: http://ism.technion.ac.il /Docs/2007/Materials-Abstracts/Poster/Drozdov.pdf
5. Wulff, F.W., Breach, C.D., Stephan, D., Saraswati, Dittmer, K.J. (2004) *Characterisation of intermetallic growth in copper and gold ball bonds on aluminium metallization*. Proceedings of 6th Electronics Packaging Technology Conference (EPTC 2004), Singapore, p. 348-353
6. *** *Semiconductor Packaging* Module II
7. http://www.npl.co.uk/, Accessed 12/01/2011